This is a preprint, the final version is subject to change, of the American Mineralogist (MSA)
Cite as Authors (Year) Title. American Mineralogist, in press.
DOI: https://doi.org/10.2138/am-2018-6599

Revision 2

# Nuwaite ($Ni_6GeS_2$) and butianite ($Ni_6SnS_2$), two new minerals from the Allende meteorite: Alteration products in the early solar system

Chi Ma* and John R. Beckett

Division of Geological and Planetary Sciences, California Institute of Technology, Pasadena, CA 91125, USA

## ABSTRACT

Nuwaite ($Ni_6GeS_2$, IMA 2013-018) and butianite ($Ni_6SnS_2$, IMA 2016-028), are two new chalcogenide minerals, occurring as micrometer-sized crystals with grossular, Na-bearing melilite, heazlewoodite, and Ge-bearing Ni-Fe alloys in veins and as mono-mineralic crack-filling material in igneous diopside in the Type B1 Ca-Al-rich inclusion (CAI) *ACM-2* from the Allende CV3 carbonaceous chondrite. The chemical composition of type nuwaite is (wt%) Ni 65.3, S 10.3, Ge 8.2, Te 7.9, Sn 5.1, and Fe 1.7, with a sum of 98.5 and an empirical formula of $(Ni_{5.95}Fe_{0.16})(Ge_{0.60}Sn_{0.23})(S_{1.72}Te_{0.33})$. The simplified formula is $Ni_6(Ge,Sn)(S,Te)_2$, leading to an end-member of $Ni_6GeS_2$. The chemical composition of type butianite is (wt%) Ni 62.1, Sn 8.9, Te 10.3, S 8.9, Ge 5.3, Fe 1.3, sum 99.1, giving rise to an empirical formula of $(Ni_{5.93}Fe_{0.13})(Sn_{0.52}Ge_{0.41})(S_{1.56}Te_{0.45})$. Butianite's simplified formula is $Ni_6(Sn,Ge)(S,Te)_2$ and the end-member formula is $Ni_6SnS_2$. Both nuwaite and butianite have an *I*4/*mmm* intergrowth structure with $a$ = 3.65Å, c = 18.14Å, $V$ = 241.7Å$^3$, and $Z$=2. Their calculated densities are 7.24 and 7.62 g/cm$^3$, respectively. Nuwaite and butianite are the first known meteoritic and solar minerals with high Ge and Sn concentrations.

Nuwaite and butianite are very late-stage, vapor-deposited, alteration products, filling in pores within preexisting grossular-rich alteration veins and cracks in igneous Al,Ti-diopside. These phases and associated heazlewoodite and Ge-bearing alloys are observed only within the Ca-, Al-rich inclusion (CAI) and not outside it or at the inclusion-matrix interface. As only sections in one half of *ACM-2* contain nuwaite/butianite, they were probably derived through a relatively low $fO_2$-

$fS_2$ sulfidation process, in which a highly-localized, low-temperature Ge-, Sn-bearing fluid interacted with a portion of the host CAI. It is likely that the fluid became relatively more Sn- and Te-enriched with time and that crack fillings post-date vein fillings, possibly due to a late remobilization of vein sulfides.

**Keywords**: Nuwaite, $Ni_6GeS_2$, butianite, $Ni_6SnS_2$, new minerals, Allende meteorite, CV3 carbonaceous chondrite, Ca-Al-rich inclusions.

*E-mail: chi@gps.caltech.edu

## INTRODUCTION

The alteration of Ca-Al-rich inclusions (CAIs) in meteorites is a story of secondary processes during the early evolution of the solar system. New secondary minerals can provide special insight because they sample special environments not encountered by most inclusions (e.g., Ma et al. 2011) or because they respond to aspects of an environment that was encountered by other phases but poorly recorded (e.g., Ma et al. 2014a). In this work, we report two new chalcogenide minerals, nuwaite ($Ni_6GeS_2$) and butianite ($Ni_6SnS_2$), which were discovered in alteration veins and filling cracks in pyroxene phenocrysts within the Type B1 CAI *ACM*-2 from the Allende CV3 chondrite. Nuwaite and butianite are the first minerals observed in meteorites that contain structurally essential Ge (nuwaite) and Sn (butianite). In addition to nuwaite and butianite, *ACM-2* is the source of three previously described new minerals, grossmanite ($CaTi^{3+}AlSiO_6$), monipite (MoNiP), and majindeite ($Mg_2Mo_3O_8$) (Ma and Rossman 2009b; Ma et al. 2014a; Ma and Beckett 2016), two of which (monipite and majindeite) are alteration phases after refractory metals.

Germanium is an unusual element in having highly variable behavior depending on physical and redox conditions (e.g., Bernstein 1985; Rouxel and Luais 2017), which can sometimes be harnessed to explore environment. For example, variations in trace Ge as a function of Ni content form the basis for classification and a delineation of fractionation processes within individual groups of iron meteorites (e.g., Scott and Wasson 1975). In terrestrial aqueous systems, Ge commonly co-precipitates in low concentrations with iron oxy(hydroxy) oxides, opaline silica, or organic material and is sometimes tapped as an environmental tracer (e.g., Bernstein 1985; Bernstein and Waychunas 1987; Froehlich et al.

1985; Kurtz et al. 2002). In hydrothermal systems, Ge (and Sn) are often present in small concentrations in sphalerite, wurtzite, and chalcopyrite (e.g., Johan 1988; Reiser et al. 2011; Frenzel et al. 2014; Evrard et al. 2015). Occasionally, Ge concentrations in a phase are high enough to produce minerals with Ge as a structurally important constituent. In rare examples, minerals with structurally important Ge are even encountered at commercially viable concentrations, the most famous example being in the oxidative alteration zone of a sulfide body at Tsumeb, Namibia (Frondel and Ito 1957; Melcher et al. 2006).

Tin, in the form of Cu-Sn alloys (i.e., bronze), is the technological basis for many early civilizations. Tin mineralization on Earth is most commonly associated with oxides from late-stage granitic liquids and low-sulfide hydrothermal fluids derived from silicic intrusions (e.g., Mlynarczyk and Williams-Jones 2006) but it can also occur in the form of tin sulfides in sulfide bodies, especially where there has been hydrothermal reworking (Evrard et al. 2015; Liu et al. 2016; Shimizu and Shikazono 1987). As noted above, Sn is often present with Ge as a minor constituent in ore sulfides such as sphalerite and it can substitute into Ge-sulfides (and *visa versa*).

Tin-enriched phases have not been previously reported in a meteorite. Germanium-bearing alloys (up to 1.7 wt% Ge; Armstrong et al. 1985b) are occasionally reported, usually associated with opaque assemblages (also known as Fremdlinge) in CAIs from carbonaceous chondrites (El Goresy et al. 1978; Wark and Lovering 1978; Armstrong et al. 1985b) but also in the R chondrite Rumuruti (Schulze et al. 1994). Armstrong et al. (1985b) described a Ge-sulfide phase with an approximate formula of $Ni_5GeS$ in an opaque assemblage from the CV3 chondrite Bali but this phase was not fully characterized. In this work, we describe the first natural occurrence of $Ni_6GeS_2$ and $Ni_6SnS_2$, as new secondary minerals in a CAI from the Allende CV3 carbonaceous chondrite. Preliminary results are given by Ma (2015a, 2017).

## MINERAL NAME AND TYPE MATERIAL

The minerals and corresponding mineral names (nuwaite, IMA 2013-018; butianite, IMA 2016-028) have been approved by the Commission on New Minerals, Nomenclature and Classification (CNMNC) of the International Mineralogical Association (Ma 2013, 2016). The names are derived from the story of "Nu Wa Bu Tian" in ancient Chinese mythology. The goddess Nu Wa patched the fractured wall of Heaven to save the early World after Pan Gu's

creation. Nuwaite was named after "Nu Wa" in allusion to this secondary mineral filling cracks in a primitive refractory inclusion in the early solar system. Butianite was named after the Chinese words "Bu Tian", meaning *patching the sky*. Butianite is the Sn-analog of nuwaite and another secondary phase that fills cracks in the same refractory inclusion in Allende.

The holotype materials for nuwaite and butianite occur within an optically-thick polished section of the CV3 carbonaceous chondrite Allende (Caltech sample Allende 12, section D2) in the type B1 CAI *ACM-2*, which is deposited under catalog # USNM 7616 in the Smithsonian Institution's National Museum of Natural History, Washington DC, USA. Butianite is restricted to this section. Nuwaite was identified in two additional sections from the Caltech collection (Allende 12, sections B2 and F) and from USNM 7554, which also sections *ACM-2*. In addition to nuwaite and butianite, holotype material for three recently described new minerals, grossmanite and monipite in section USNM 7554 and majindeite in section USNM 7615, are present in the same CAI (Ma and Rossman 2009b; Ma et al. 2014a; Ma and Beckett 2016).

## OCCURRENCE

The Allende meteorite fell in and near Pueblito de Allende, Chihuahua, Mexico on February 8, 1969 (Clarke et al. 1971). It is a CV3 carbonaceous chondrite and, due to the large amount of fresh material (total known weight ~ 2 tons), is probably the most heavily studied meteorite in existence; results from the study of Allende samples have greatly influenced current thinking about processes, timing, and chemistry in the primitive solar nebula and in small planetary bodies. Moreover, Allende continues to be a source of information for new-to-science materials produced in the early solar system more than four decades after its fall (e.g., Ma et al. 2014b; Ma 2015b). Nuwaite and butianite are just two of nineteen new minerals discovered in Allende since 2007.

Coarse-grained CAIs are classically divided according to mineralogy and mode into types A (melilite dominant), B (subequal amounts of clinopyroxene + melilite), and C (significant amounts of anorthite). Types B1 and B2 inclusions are distinguished by the presence (B1) or absence (B2) of a melilite-rich mantle. In general, coarse-grained CAIs are characterized by high concentrations of elements that are refractory in a cooling gas of solar composition and in ratios suggesting that they captured the ~4% most condensable elements from a gas of solar composition (e.g., Grossman and Ganapathy 1976).

The minerals nuwaite and butianite are present within the CAI, *ACM-2*, which was serially sectioned from a ~1 cm diameter fragment of Allende (Caltech Meteorite Collection No. Allende12A). Ma and Rossman (2009b) and Ma et al. (2014a) provide petrographic descriptions of the inclusion and its constituent phases. Only a small portion of a once much larger inclusion bounded by a matrix of mostly fine-grained olivine and troilite still exists in fragment 12A and, therefore, sections of it, which leads to ambiguity concerning the nature of the host inclusion. Ma et al. (2014a) argued, based primarily on geometric considerations and the presence of low-Ti clinopyroxene phenocrysts, that *ACM-2* was a large type B1 CAI, ~7 mm in diameter, and that the presence of a Wark-Lovering rim where the inclusion contacts matrix implies that the remaining material is a portion of the melilite-rich mantle. We accept this designation in the present work and refer the reader to Ma and Rossman (2009b), Ma et al. (2014a), and Ma and Beckett (2016) for additional mineral compositions and a general petrographic description of this inclusion. All of the observed nuwaite and butianite occurs in sections from one half of *ACM-2*. This localization of occurrence points to a correspondingly localized source of Ge and Sn within or outside the CAI, and/or a precipitation/condensation process dictated by localized conditions within the CAI.

Figure 1a shows a back-scatter electron (BSE) image of the region containing the holotype material for both of the new minerals. Locations of type nuwaite and butianite are indicated. The type nuwaite occurs ~700 μm from the rim of *ACM-2* in a grossular-rich vein that also contains Na-bearing melilite and Ge-bearing Ni-Fe alloy (Fig. 1b). Host melilite is ~Ak24. Nuwaite is also found filling cracks in Al,Ti-diopside within 300-600 μm of the Wark-Lovering rim. Type butianite is ~350 μm from the Wark-Lovering rim and occurs in cracks within one Al,Ti-diopside crystal (Fig. 1c).

## APPEARANCE, PHYSICAL, AND OPTICAL PROPERTIES

Nuwaite occurs as irregular grains, 1-6 μm in size (Figs. 1b). Butianite occurs as irregular grains, 0.5 to 1.4 μm in width and 1-8 μm long, the longest, shown in Fig. 1c, occurs in a crack. Both minerals are opaque. Color, luster, streak, hardness, tenacity, cleavage, fracture, density, and optical properties could not be determined because of the small grain size. The density, calculated from its crystal structure and the empirical formula, as described below, is 7.24 g/cm$^3$ for nuwaite, and 7.62 g/cm$^3$ for butianite.

## ANALYTICAL TECHNIQUES

Chemical analyses of nuwaite and butianite were carried out using a JEOL 8200 electron microprobe interfaced with the Probe for EPMA program from Probe Software, Inc. and operated in focused beam mode at 15 kV or 10 kV and 10 nA. Quantitative elemental microanalyses were processed with the PAP correction procedure (Pouchou and Pichoir 1991) and analytical results are given in Table 1. Standards were Ni, Ge, Sn, Te, Co, Pt, and Ru metals and $FeS_2$ (for Fe and S). An Oxford INCA X-ray energy dispersive spectrometer (EDS) on a ZEISS 1550VP field emission SEM was also used for elemental analysis of associated alloys, sulfides, oxides and silicates. These data were processed using the XPP correction procedure of Pouchou and Pichoir (1991) and Oxford factory internal standards. Electron back-scatter diffraction (EBSD) analyses were obtained using an HKL EBSD system mounted on the ZEISS 1550VP field emission SEM. Details of operating conditions for EBSD are given below.

## CHEMICAL COMPOSITION

The type nuwaite (Fig. 1a & 1b) has an empirical formula of $(Ni_{5.95}Fe_{0.16})(Ge_{0.60}Sn_{0.23})(S_{1.72}Te_{0.33})$ with a simplified formula of $Ni_6(Ge,Sn)(S,Te)_2$. The end-member formula for nuwaite is $Ni_6GeS_2$, which requires (wt%) Ni 72.03, Ge 14.85, S 13.12, total 100 wt%. The type butianite (Fig. 1a & 1c) has an empirical formula of $(Ni_{5.93}Fe_{0.13})(Sn_{0.52}Ge_{0.41})(S_{1.56}Te_{0.45})$. Here, the simplified formula is $Ni_6(Sn,Ge)(S,Te)_2$ with an end-member formula of $Ni_6SnS_2$, which requires (wt%) Ni 65.83, Sn 22.18, S 11.99, for a total of 100.00. Observed compositions of nuwaite-butianite in *ACM-2* span a range in Ge# [100*Ge/(Ge + Sn) on a molar basis] from 10-90 (Fig. 2a). Given that the endmember $Ni_6SnS_2$ is stable at 540°C (Baranov et al. 2003), there is likely to be a complete solid-state solution between nuwaite and butianite over some temperature range. Tellurium/sulfur ratios are also variable, ranging over a factor of three (0.1 – 0.3). The most Te-enriched nuwaite-butianite in *ACM-2* are crack-filling butianites (Fig. 2c) and the most Te-depleted are Ge-rich nuwaites in sections that contain no butianite (Fig. 2b). We note that the Ge-sulfide described by Armstrong et al. (1985b), $(Ni,Fe,Co)_{5.00}(Ge,Sn)_{0.94}(S,Te)_{1.00}$ has a molar (Ge+Sn)/(S+Te) = 0.9 that is much higher than expected for nuwaite, ~0.5. Moreover, (Ni+Fe+Co)/Ge = 5.2 with very low Sn is significantly lower than expected for a Sn-poor nuwaite (≥ 6). The Armstrong et al. phase is not

nuwaite. It may be related to $Ni_9Ge_2S_2$ (Ni/Ge =4.5), which would be the Ge-analog of $Ni_9Sn_2S_2$, a known synthetic material (Baranov et al. 2003). Butianite may be related to an unnamed mineral with a formula of $(Ni,Cu,Fe,Co)_{5.43}(Sn,Sb)_{1.04}(S,Te)_{2.00}$ that was observed as an inclusion in heazlewoodite from a serpentinized peridotite by Hudson and Travis (1981). However, the Ni+Cu+Fe+Co content appears to be too low for a butianite.

## COEXISTING PHASES

Ma and Rossman (2009b), Ma et al. (2014a), and Ma and Beckett (2016) give compositions of the major igneous phases in *ACM-2* and of various phases associated with the Mo-oxides majindeite and kamiokite. Nuwaite occurs with grossular $[(Ca_{2.92}Mn_{0.07})Al_{2.02}Si_{2.99}O_{12}]$, Na-bearing melilite $[(Ca_{1.82}Na_{0.14})Al_{0.99}(Si_{1.23}Al_{0.77})O_7]$, Fe-, Zn-bearing spinel $[(Mg_{0.92}Fe_{0.05}Zn_{0.03})Al_2O_4]$, and Ge-bearing Ni-Fe alloys (e.g., $Ni_{0.82}Fe_{0.12}Ge_{0.02}Co_{0.02}Pt_{0.02,}$ $Ni_{0.83}Fe_{0.11}Co_{0.03}Ge_{0.01}$) in alteration veins within igneous melilite (~Ak24), or filling cracks alone in melilite or Al-, Ti-diopside. Butianite only occurs within cracks in Al-, Ti-rich diopside $[Ca_{1.01}(Mg_{0.46}Al_{0.31}Ti^{4+}_{0.14}Ti^{3+}_{0.08})(Si_{1.43}Al_{0.57})O_6]$, which also contain nuwaite, heazlewoodite ($Ni_3S_2$), Ge-bearing Ni-Fe alloy ($Ni_{0.84}Fe_{0.12}Ge_{0.02}Co_{0.01}$) and, possibly, monticellite ($CaMgSiO_4$). Representative analyses of Ge-bearing alloys and of heazlewoodite are given in Table 1. Note that the alloy composition is at the Ni-rich extreme for *ACM-2*, consistent with late-stage alteration and not with likely Fe-rich condensates (Ma and Beckett 2016). Heazlewoodite and Ni-rich alloys are usually isolated but are occasionally observed in contact.

## CRYSTALLOGRAPHY

Conventional X-ray studies could not be carried out on either nuwaite or butianite because of the small crystal and aggregate size. We were, however, able to obtain EBSD analyses at a submicrometer scale on the vibration-polished section USNM 7616 using methods described in Ma and Rossman (2008, 2009a). An HKL (now Oxford) EBSD system on a Zeiss 1550VP scanning electron microscope was used for these measurements and operated at 20 kV and 6 nA in a focused beam configuration with a 70º tilted stage and variable pressure (25 Pa) mode. The EBSD system was calibrated using a single-crystal silicon standard, an approach that allows the study of uncoated specimens. The structures of nuwaite and butianite were determined

and cell parameters obtained by matching the observed EBSD patterns with structures of synthetic $Ni_6SnS_2$ and $Ni_9Sn_2S_2$ (Baranov et al. 2003), and synthetic $Ni_{8.21}Ge_2S_2$ and $Ni_{8.45}Ge_2Se_2$ (Isaeva et al. 2009).

The EBSD patterns of both nuwaite and butianite (Fig. 3) match well to the tetragonal *I*4/*mmm* $Ni_6SnS_2$ superstructure (Baranov et al. 2003) with mean angular deviations of 0.33 º to 0.39º. The corresponding cell parameters are $a$ = 3.650 Å, $c$ = 18.141 Å, V = 241.68 Å$^3$, and Z = 2. To our knowledge, nuwaite has not been synthesized. It is, however, isostructural with synthetic $Ni_6SnS_2$, so a description based on Baranov et al.'s (2003) study of butianite suffices for both phases. The crystal structure of nuwaite-butianite is characterized by alternating layers of metal, $Ni_5$(Ge,Sn) in a $Cu_3Au$-type configuration, with two crystallographically distinct $Ni_{0.5}S$ slabs. Roughly equal amounts of each type of $Ni_{0.5}S$ slab are stacked statistically perpendicular to the crystallographic $c$-axis. Only ¼ of the possible Ni sites in any given slab are occupied with Ni, which forms either distorted NaCl- or $Li_2O$-arrangements with S. NaCl-, $Li_2O$-, and $Cu_3Au$-type building blocks are observed in a broad range of chalcogenides (e.g., Baranov et al. 2003; Isaeva et al. 2009; Kuznetsov et al. 2017). The physical properties of nuwaite and butianite have not been studied but, based on the metal-sulfide layering, they are likely to be strongly anisotropic.

X-ray powder-diffraction data (in Å for Cu*K*α1, Bragg-Brentano geometry) are calculated from the cell parameters from Baranov et al. (2003) with the empirical formula of type nuwaite and butianite from this study, using Powder Cell version 2.4. The strongest calculated X-ray powder diffraction lines [d in Å, (I), *hkl*] are 4.535 (100) (*004*), 3.024 (9) (*006*), 1.963 (10) (*116*), 1.825 (31) (*200*), 1.704 (10) (*118*), 1.693 (24) (*204*), 1.291 (10) (*220*) for nuwaite, and 4.535 (100) (*004*), 3.024 (12) (*006*), 1.963 (14) (*116*), 1.825 (38) (*200*), 1.704 (10) (*118*), 1.693 (30) (*204*), 1.291 (12) (*220*), 1.241 (11) (*224*) for butianite.

## DISCUSSION

Germanium and tin commonly substitute together as minor constituents in sulfides such as sphalerite and chalcopyrite (e.g., Gill et al. 2016; Maiken et al. 2003; Reiser et al. 2011) but they also form sulfides wherein Ge or Sn is structurally required and there are several natural sulfides for which there are isostructural Ge and Sn end-member minerals: argyrodite - canfieldite [$Ag_8$(Ge,Sn)$S_6$]; briartite - stannite [($Cu_2Fe$(Ge,Sn)$S_4$]; germanite - ferrokesterite

250 [$(Cu_{26}Fe_4(Ge,Sn)_4S_{32}$]; omariniite - stannoidite [$Cu_6^{+}Cu_2^{+2}(Fe,Zn)(Ge,Sn)S_{12}$]. Reported
251 descriptions of these phases tend to be either Ge- or Sn-enriched but intermediate compositions
252 do occur for some pairs, suggesting that complete solid solutions may exist. Nuwaite – butianite
253 [$Ni_6(Ge,Sn)S_2$] represents a new Ge-Sn sulfide solid solution. Compositions of nuwaite-
254 butianite in *ACM-2* have Ge#s from 10 – 90%, consistent with a complete solid solution under
255 the conditions encountered in that inclusion. The large range in Ge/Sn in nuwaite-butianite
256 directly reflects differences in Ge/Sn in the local fluid, although equilibrium constants relating
257 these ratios are currently unknown. Nuwaite and butianite are the first known meteoritic
258 minerals with high Ge and Sn concentrations. In the following paragraphs, we explore the
259 significance of sulfides and alloys in *ACM-2* and place nuwaite-butianite within the framework
260 of Fe-Ni-S evolution in this and other CAIs.
261 Type B1 inclusions like *ACM-2* were partially to completely melted one or more times
262 under reducing conditions with volatilization that led to crystallization of a melilite-rich mantle
263 (Mendybaev et al. 2006; MacPherson 2014). One might reasonably expect concentrations of
264 moderately to highly volatile elements to be depleted in such objects but there is abundant
265 evidence that many CAIs have relatively high concentrations of relatively volatile elements.
266 These features of the bulk chemistry are thought to indicate secondary processing at low
267 temperatures, either in the solar nebula or on parent bodies (e.g., Krot et al. 1995; MacPherson
268 2014). We are not aware of bulk Ge concentrations for CAIs or their components but some data
269 are available for Sn. These data show that, on average, bulk Sn concentrations in Allende CAIs
270 are only depleted by a factor of two relative to bulk Allende (Mason and Martin 1977; Fehr et al.
271 2009).
272 Germanium and tin are moderately volatile elements in a nebular setting (Lodders 2003),
273 although this follows from an assumption that Fe-Ge and Fe-Sn alloys form ideal solutions.
274 Given the low predicted condensation temperatures, even referenced to a high nebular pressure
275 {[577°C(Sn)-597°C(Ge) for a total pressure of $10^{-3}$ atm]; Lodders 2003}, nonideality and
276 magnetic contributions to the free energy are likely important (e.g., Capobianco et al. 1999; Hari
277 Kumar et al. 1998). These factors could be sufficient to change the order of condensation (i.e.,
278 make Ge more volatile than Sn) but they do not obviate the basic conclusion that both Ge and Sn
279 are moderately volatile elements in a nebular setting and that the formation of nuwaite-butianite,
280 if nebular, occurred at low temperatures. Thus, they are not part of the high-temperature

melting/evaporation event(s) that led to the formation of the refractory igneous portions of *ACM-2*. The localized distribution of nuwaite-butianite might seem to argue against a strictly nebular origin because a nebular vapor would have had access to the entire surface of the CAI. One might, therefore, expect nuwaite-butianite to be broadly distributed in cracks and veins throughout *ACM-2* and not restricted a small portion of the inclusion. However, Ma and Beckett (2016) pointed out that Ni enrichment in alloys from *ACM-2* reflected local exhaustion of magnetite in opaque assemblages. Local environments within the CAI were dictated by the local presence or absence of magnetite-bearing phase assemblages with easy access to local cracks and veins. Volatilization of high S phases similarly fed the local vapor and their exhaustion would have led to locally low S fugacities. The presence of heazlewoodite and Ge-bearing Ni-rich alloys only in sections that contain nuwaite-butianite could, in fact, be consistent with a nebular environment.

In *ACM-2*, nuwaite-butianite and associated Ge-bearing, Ni-rich alloys and heazlewoodite occur in existing alteration veins and cracks that post-date all melting events, which implies a low-temperature origin. The range of sulfide-bearing phase assemblages suggests a large range in $fS_2$. The sulfur-rich phase molybdenite ($MoS_2$; sulfur/metal = 2) and pentlandite [$(Fe,Ni)_9S_8$; sulfur/metal = 0.9] are observed in one opaque assemblage, where the evolution of the phase assemblage is largely constrained by the presence or absence of magnetite as discussed by Ma and Beckett (2016). Heazlewoodite ($Ni_3S_2$; sulfur/metal = 0. 7) is the most common sulfide in veins and cracks in *ACM-2* and $fS_2$ values for heazlewoodite plus awaruite are lower than those needed to stabilize pentlandite (e.g., Alt and Shank 1998). Nuwaite-butianite is even less S-rich than heazlewoodite (sulfur/metal = 0.3). From Baranov et al. (2003), butianite + heazlewoodite + alloy is a stable phase assemblage at 540°C. This implies that butianite is limited to $fS_2$ values equal to or lower than those needed to stabilize heazlewoodite + alloy (e.g., $2Ni_3S_2 + Ge = Ni_6GeS_2 + S_2$ at the same temperature). The presence of incompatible sulfides in *ACM-2* implies that the degree of reaction varies locally. Overall, the process is one of reduction and volatilization of Fe and S with sulfide/metal ratios decreasing progressively as S is stripped from the sulfides. There are abundant examples of disequibrium over the short spatial scales offered by *ACM-2* (e.g., monipite-tugarinovite and apatite; the presence of molybdenite and pentlandite + magnetite in the same inclusion that has kamiokite+awaruite and heazlewoodite+alloy) have been described by Ma et al. (2014a) and Ma and Beckett (2016).

Although the specific Ge-sulfide for the occurrence of Armstrong et al. (1985b) is unknown, it has a similar key phase assemblage (i.e., Ge-sulfide, heazlewoodite, Ni-rich alloy), so that a similar origin is implied. Equilibria such as $2Ni_6GeS_2$(nuwaite) + $S_2$ = $Ni_5GeS_2$(Armstrong phase) +$Ni_3S_2$(heazlewoodite) presumably control which chalcogenide appears. The higher sulfur/Ni ratio for the Armstrong et al. (1985b) phase suggests that it requires a higher $fS_2$ than does nuwaite.

For both nuwaite and butianite, the source of the Ge and Sn, as well as the significant concentrations of Te, is problematic. We observed no potential Sn- or Ge-source phases in or immediately outside *ACM-2* but the fact that nuwaite occurs in only one half of the CAI implies a local source or a unique fluid altering phase assemblage that caused precipitation. Given that type B1 inclusions are relatively common in Allende and nuwaite-butianite has been observed in only one (i.e., *ACM-2*), it seems likely that the source of the Ge, Sn, and Te is external to the CAI. We also note that nuwaite and butianite are not observed outside the Wark-Lovering rim (i.e., in the matrix) but nuwaite is observed inside multiple sections of *ACM-2* (Sn concentrations are high enough for butianite only in one section). This suggests that the source (or the transport medium) was highly localized. Ge-bearing alloys have been previously reported (Armstrong et al. 1985a; El Goresy et al. 1978; Wark and Lovering 1978) but these are usually associated with opaque assemblages and were likely produced as part of the oxidation-sulfidation processes that affected these objects (e.g., Armstrong et al. 1985a; 1987; Blum et al. 1989). *ACM-2* was extensively metasomatized such that the stable Fe-Ni alloys became extremely Ni-rich and Ni-sulfides appeared. Sulfur-rich sulfides like pentlandite and molybdenite are rare in *ACM-2* and troilite is not observed. Heazlewoodite is generally not observed in Allende CAIs but it is the most common sulfide in veins of *ACM-2* although it appears only in sections containing nuwaite-butianite. Germanium- and Sn-chalcogenides have only been reported in *ACM-2* and a CAI from Bali (Armstrong et al. 1985b). In most sulfidized CAIs, nuwaite and butianite are not observed because the $fS_2$ was too high and in sulfide-free CAIs, the local $fS_2$ was too low.

Butianite was synthesized by Baranov et al. (2003) at 540°C in the system Ni-Sn-S. They observed a stable field for butianite - Ni metal – heazlewoodite, which is the collection of phases observed in *ACM-2*, albeit with significant Fe in the alloy and no example of all three phases in contact. However, neither upper nor lower temperature limits on the stability of butianite (or nuwaite) are known. Thus, just how low a temperature might be represented by

nuwaite-butianite is difficult to quantify based on the available data. Where Ge- and Sn-sulfides are observed in terrestrial rocks, emplacement temperatures in the range of 200-400°C have been inferred (Chetty and Frimmel 2000; Melcher et al. 2006; Shimizu and Shikazano 1987).

Taking aside the unnamed mineral described by Hudson and Travis (1981), the closest terrestrial analog for heazlewoodite and nuwaite-butianite in *ACM-2* would seem to be the heazlewoodite-awaruite assemblage commonly observed in serpentinized peridotites (Alt and Shanks 1998; Eckstrand 1975; Gole 2014; Klein and Bach 2009; Sciortino et al. 2015; Tzamos et al. 2016; Williams 1960). Serpentinization of mafic and ultramafic rocks is a large-scale, on-going process in oceanic environments. Here, large volumes of ocean water oxidize $Fe^{2+}$ from silicates, releasing $H_2$, which creates reducing conditions. Where the water-rock ratio is high, these reduced fluids strip S and Fe from sulfides so that stable heazlewoodite-awaruite is produced at 200-300° and relatively shallow depths. The assemblage reflects low $fS_2$ and relatively (for a terrestrial system) low $fO_2$ (see Fig. 8 of Alt and Shanks 1998). The nature of the fluid that produced nuwaite-butianite is poorly constrained. The lack of hydrated phases in *ACM-2* suggests that this was not an aqueous solution at near-ambient temperatures.

The presence of significant concentrations of Te in nuwaite-butianite also provides a clue to origin because Te is generally more volatile than S in terrestrial environments and tellurides are generally very late stage products. From Fig. 2, Te/S is generally higher in cracks than in veins and it increases with increasing Sn/Ge. It is likely that increasing Te/S is associated with lower temperatures and, since Te/S correlates with Sn/Ge, it follows that butianite is probably a lower temperature phase than nuwaite and that crack filling nuwaite-butianite post-dates vein-filling nuwaite.

## IMPLICATIONS

Nuwaite and butianite are opportunistic late-stage alteration products that fill pores and fractures in an Allende CAI. Their absence in most other CAIs is likely due to the high $fS_2$ governed by S-rich phases like pentlandite that are incompatible with low-S chalcogenides like nuwaite-butianite. They formed after the commonly observed secondary grossular in alteration veins and are likely vapor-deposited phases at low temperatures. Nuwaite-butianite reflect the last stage of alteration for *ACM-2*. Sn-Te enrichment occurred at lower temperatures than Ge (i.e., butianite is later) with balancing of low $fS_2$ with high enough temperature and Ni.

374 Nuwaite-butianite is an end-stage condensate produced during desulfurization of a
375 CAI. Generally, this process does not proceed in most CAIs to the point where
376 heazlewoodite and nuwaite-butianite are stabilized, so these phases are rare. Nuwaite also
377 represents a previously unknown material and may be exploited for developing functional
378 materials with intergrowth structures.
379
380 **ACKNOWLEDGEMENTS**

381 SEM, EBSD and EPMA analyses were carried out at the Caltech GPS Division
382 Analytical Facility, which is supported, in part, by NSF Grants EAR-0318518 and DMR-
383 0080065. JRB acknowledges NASA grant NNG04GG14G. We thank Klaus Keil, Mike
384 Zolensky and associate editor Steven Simon for helpful reviews.
385
386 **REFERENCES**

387 Alt, J.C. and Shanks, W.C. (1998) Sulfur in serpentinized oceanic peridotites: Serpentinization
388 processes and microbial sulfate reduction. Journal of Geophysical Research, 103, 9917-
389 9929.
390 Armstrong, J.T., El Goresy, A., and Wasserburg, G.J. (1985a) Willy: A prize noble Ur-
391 Fremdling—Its history and implications for the formation of Fremdlinge and CAI.
392 Geochimica et Cosmochimica Acta, 49, 1001-1022.
393 Armstrong, J.T., Hutcheon, I.D., and Wasserburg, G.J. (1985b) Ni-Pt-Ge-rich Fremdlinge:
394 Indicators of a turbulent early solar nebula. Meteoritics, 20, 603A-605A.
395 Armstrong, J.T., Hutcheon, I.D., and Wasserburg, G.J. (1987) Zelda and company: Petrogenesis
396 of sulfide-rich Fremdlinge and constraints on solar nebula processes. Geochimica et
397 Cosmochimica Acta 51, 3155-3173.
398 Baranov, A.I., Isaeva, A.A., Kloo, L., and Popovkin, B.A. (2003) New metal-rich sulfides
399 $Ni_6SnS_2$ and $Ni_9SnS_2$ with a 2D metal framework: synthesis, crystal structure, and bonding.
400 Inorganic Chemistry, 42, 6667–6672.
401 Bernstein, L.R. (1985) Germanium geochemistry and mineralogy. Geochimica et Cosmochimica
402 Acta, 49, 2409-2422.

Bernstein, L.R. and Waychunas, G.A. (1987) Germanium crystal chemistry in hematite and goethite from the Apex Mine, Utah, and some new data on germanium in aqueous solution and in stottite. Geochimica et Cosmochimica Acta, 51, 623-630.

Blum, J.D., Wasserburg, G.J., Hutcheon, I.D., Beckett, J.R., and Stolper, E.M. (1989) Origin of opaque assemblages in C3V meteorites: Implications for nebular and planetary processes. Geochimica et Cosmochimica Acta, 53, 543-556.

Capobianco, C.J., Drake, M.J., and de'Aro, J. (1999) Siderophile geochemistry of Ga, Ge, and Sn: Cationic oxidation states in silicate melts and the effect of composition in iron-nickel alloys. Geochimica et Cosmochimica Acta, 63, 2667-2677.

Chetty, D. and Frimmel, H.E. (2000) The role of evaporates in the genesis of base metal sulphide mineralisation in the Northern Platform of the Pan-African Damara Belt, Namibia: geochemical and fluid inclusion evidence from carbonate wall rock alteration. Mineralium Deposita 35, 364-376.

Clarke, R.S., Jarosewich, E., Mason, B., Nelen, J., Gomez, M., and Hyde, J.R. (1971) The Allende, Mexico, meteorite shower. Smithsonian Contributions to the Earth Science, 5, 1–53.

Eckstrand, O.R. (1975) The Dumont serpentinite: A model for control of nickeliferous opaque mineral assemblages by alteration reactions in ultramafic rocks. Economic Geology, 70, 183-201.

El Goresy, A., Nagel, K, and Ramdohr, P. (1978) Fremdlinge and their noble relatives. Proceedings of the Lunar and Planetary Science Conference, 9, 1279-1303.

Evrard, C., Fouquet, Y., Moëlo, Y., Rinnert, E., Etoubleau, J., and Langlade, J.A. (2015) Tin concentration in hydrothermal sulphides related to ultramafic rocks along the mid-Atlantic Ridge: a mineralogical study. European Journal of Mineralogy, 27, 627-638.

Fehr, M.A., Rehkämper, M., Halliday, A.N., Hattendorf, B., and Günther, D. (2009) Tellurium isotope compositions of calcium-aluminum-rich inclusions. Meteoritics & Planetary Science, 44, 971-984.

Frenzel, M., Ketris, M.P., and Gutzmer, J. (2014) On the geological availability of germanium. Mineralium Deposita, 49, 471-486.

Froehlich, P.N., Hambrick, G.A., Andreae, M.O., Mortlock, R.A., and Edmond, J.M. (1985) The geochemistry of inorganic germanium in natural waters. Journal of Geophysical Research, 90, 1133-1141.

Frondel, C. and Ito, J. (1957) Geochemistry of germanium in the oxidized zone of the Tsumeb Mine, south-west Africa. American Mineralogist, 42, 743-753.

Gill, S.B., Piercey, S.J., and Layton-Matthews, D. (2016) Mineralogy and metal zoning of the Cambrian Zn-Pb-Cu-Ag-Au Lemarchant volcanogenic massive sulfide (VMS) deposit, Newfoundland. Canadian Mineralogist, 54, 1307-1344.

Gole, M.J. (2014) Leaching of S, Cu, and Fe from disseminated Ni-(Fe)-(Cu) sulphide ore during serpentinization of dunite host rocks at Mount Keith, Agnew-Wiluna belt, western Australia. Mineralium Deposita, 49, 821-842.

Grossman, L. and Ganapathy, R. (1976) Trace elements in the Allende meteorite—Coarse-grained, Ca-rich inclusions. Geochimica et Cosmochimica Acta, 40, 331-344.

Hari Kumar, K.C., Wollants, P., and Delaey, L. (1996) Thermodynamic evaluation of Fe-Sn phase diagram. Calphad, 20, 139-149.

Hudson, D.R. and Travis, G.A. (1981) A native nickel-heazlewoodite-ferroan trevorite assemblage from Mount Clifford, western Australia. Economic Geology, 76, 1686-1697.

Isaeva, A.A., Baranov, A.I., Kloo, L., Ruck, M. and Popovkin, B.A. (2009) New metal-rich mixed chalcogenides with intergrowth structures: $Ni_{8.21}Ge_2S_2$ and $Ni_{8.45}Ge_2Se_2$. Solid State Sciences, 11, 1071–1076.

Johan, Z. (1988) Indium and germanium in the structure of sphalerite: an example of coupled substitution with copper. Mineralogy and Petrology, 39, 211–229.

Klein, F. and Bach, W. (2009) Fe-Ni-Co-O-S phase relations in peridotite-seawater interactions. Journal of Petrology, 50, 37–59.

Krot, A.N., Scott, E.R.D., and Zolensky, M.M. (1995) Mineralogical and chemical modification of compnents in CV3 chondrites: Nebular or asteroidal? Meteoritics, 30, 748–775.

Kurtz, A.C., Derry, L.A., and Chadwick, O.A. (2002) Germanium-silicon fractionation in the weathering environment. Geochimica et Cosmochimica Acta 66, 1525–1537.

Kuznetsov, A.N., Stroganova, E.A., Serov, A.A., Kirdyankin, D.I., and Novotortsev, V.M. (2017) New quasi-2D nickel-germanium mixed chalcogenides based on the $Cu_3Au$-type extended fragments. Journal of Alloys and Compounds, 696, 413–422.

Liu, W., Cook, N.J., Ciobanu, C.L., Liu, Y., Qiu, X., and Chen, Y. (2016) Mineralogy of tin-sulfides in the Zijnshan porphyry-epithermal system, Fujian province, China. Ore Geology Reviews, 72, 682–698.

Lodders, K. (2003) Solar system abundances and condensation temperatures of the elements. Astrophysical Journal, 591, 1220-1247.

Ma, C. (2013) Nuwaite, IMA 2013-018. CNMNC Newsletter No. 16, August 2013, page 2704. Mineralogical Magazine, 77, 2695–2709.

Ma, C. (2015a) Discovery of nuwaite, $Ni_6GeS_2$, a new alteration mineral in Allende. Meteoritics & Planetary Science, 50 (S1), No. 5151.

Ma, C. (2015b) Nanomineralogy of meteorites by advanced electron microscopy: Discovering new minerals and new materials from the early solar system. Microscopy and Microanalysis, 21 (Suppl 3), 2353–2354. DOI:10.1017/S1431927615012544

Ma, C. (2016) Butianite, IMA 2016-028. CNMNC Newsletter No. 32, August 2016, page 920, Mineralogical Magazine, 80, 915–922.

Ma, C. (2017) Discovery of new mineral butianite, $Ni_6SnS_2$, an alteration phase from Allende. Meteoritics & Planetary Science, 52 (S1), No. 6032.

Ma, C. and Beckett, J.R. (2016) Majindeite, $Mg_2Mo_3O_8$, a new mineral from the Allende meteorite and a witness to post-crystallization oxidation of a Ca-Al-rich refractory inclusion. American Mineralogist, 101, 1161-1170.

Ma, C. and Rossman, G.R. (2008) Barioperovskite, $BaTiO_3$, a new mineral from the Benitoite Mine, California. American Mineralogist, 93, 154–157.

Ma, C. and Rossman, G.R. (2009a) Tistarite, $Ti_2O_3$, a new refractory mineral from the Allende meteorite. American Mineralogist, 94, 841–844.

Ma, C. and Rossman, G.R. (2009b) Grossmanite, $CaTi^{3+}AlSiO_6$, a new pyroxene from the Allende meteorite. American Mineralogist, 94, 1491–1494.

Ma, C., Connolly, H.C., Beckett, J.R., Tschauner, O., Rossman, G.R., Kampf, A.R., Zega, T.J., Sweeney Smith, S.A., and Schrader, D.L. (2011) Brearleyite, $Ca_{12}Al_{14}O_{32}Cl_2$, a new alteration mineral from the NWA 1934 meteorite. American Mineralogist, 96, 1199–1206.

Ma, C., Beckett. J.R., and Rossman, G.R. (2014a) Monipite, MoNiP, a new phosphide mineral in a Ca-Al-rich inclusion from the Allende meteorite. American Mineralogist, 99, 198–205.

493 Ma, C., Beckett. J.R., and Rossman, G.R. (2014b) Allendeite ($Sc_4Zr_3O_{12}$) and hexamolybdenum
494 (Mo,Ru,Fe), two new minrals from an ultrarefractory inclusion from the Allende
495 meteorite. American Mineralogist, 99, 654–666.
496 MacPherson, G.J. (2014) Calcium-aluminum-rich inclusions in chondritic meteorites., p. 201-
497 246 in A.M. Davis (ed.) Treatise on Geochemistry, volume 1. Elsevier.
498 Maiken, K.I., Hansen, K., Mokovicky, E., and Karup-Møller, S. (2003) Exploratory studies on
499 substitutions in tetrahedrite–tenantite solid-solution. Part IV. Substitution of germanium and
500 tin. Neues Jahrbuch für Mineralogie Abhandlung, 179, 43–71.
501 Mason, B. and Martin, P.M. (1977) Geochemical differences among components of the Allende
502 meteorite. Smithsonian Contributions to the Earth Sciences, 19, 84–95.
503 Melcher, F., Oberthür, T., and Rammlmair, D. (2006) Geochemical and mineralogical
504 distribution of germanium in the Khusib Springs Cu-Zn-Pb-Ag sulfide deposit, Otavi
505 Mountain Land, Namibia. Ore Geology Reviews, 28, 32–56.
506 Mendybaev, R.A., Richter, F.M., and Davis, A.M. (2006) Crystallization of melilite from
507 CMAS-liquids and the formation of the melilite mantle of type B1 CAIs: Experimental
508 simulations. Geochimica et Cosmochimica Acta, 70, 2622–2642.
509 Mlynarczyk, M.S.J. and Williams-Jones, A.E. (2006) Zoned tourmaline associated with
510 cassiterite: Implications for fluid evolution and tin mineralization in the San Rafael Sn–
511 deposit, southeastern Peru. Canadian Mineralogist, 44, 347–365.
512 Pouchou, J.-L. and Pichoir, F. (1991) Quantitative analysis of homogeneous or stratified
513 microvolumes applying the model "PAP". In Electron Probe Quantitation (Heinrich, K.F.J.
514 and Newbury, D.E., eds.), Plenum Press, 31–75.
515 Reiser, F.K.M., Rosa, D.R.N., Pinto, A.M.M., Carvalho, J.R.S., Matos, J.X., Guimarães, F.M.G.,
516 Alves, L.C., and de Oliveira, D.P.S. (2011) Mineralogy and geochemistry of tin- and
517 germanium-bearing copper ore, Barrigão re-mobilized vein deposit, Iberian pyrite belt,
518 Portugal. International Geology Review, 53, 1212–1238.
519 Rouxel, O.J. and Luais, B. (2017) Germanium isotope geochemistry. Reviews in Mineralogy and
520 Geochemistry, 82, 601–656.
521 Schulze, H., Bischoff, A., Palme, H., Spettel, B., Dreibus, G., and Otto, J. (1994) Mineralogy and
522 chemistry of Rumuruti: The first meteorite fall of the new R chondrite group. Meteoritics,
523 29, 275–86.

524 Sciortino, M., Mungall, J.E., and Muinonen, J. (2015) Generation of high-Ni sulfide and alloy
525 phases during serpentinization of dunite in the Dumont sill, Quebec. Economic Geology,
526 110, 733–761.
527 Scott, E.R.D. and Wasson, J.T. (1975) Classification and properties of iron meteorites. Reviews
528 of Geophysics and Space Physics, 13, 527–546.
529 Shimizu, M. and Shikazono, N. (1987) Stannoidite-bearing tin ore: mineralogy, texture and
530 physiochemical environment of formation. Canadian Mineralogist, 25, 229–236.
531 Tzamos, E., Filippidis, A., Michailidis, K., Koroneos, A., Rassios, A., Grieco, G., Pedrotti, M.,
532 and Stamoulis, K. (2016) Mineral chemistry and formation of awaruite and heazlewoodite in
533 the Xerolivado chrome mine, Vourinos, Greece. Bulletin of the Geological Society of
534 Greece, 50, 2047–2056.
535 Wark, D.A. and Lovering J.F. (1978) Refractory/platinum metals and other opaque phases in
536 Allende Ca-Al-rich inclusions (CAI's). Lunar and Planetary Science, 9, 1214–1216.
537 Williams, K.L. (1960) An association of awaruite with heazlewoodite. American Mineralogist,
538 45, 450–453.
539

This is a preprint, the final version is subject to change, of the American Mineralogist (MSA)
Cite as Authors (Year) Title. American Mineralogist, in press.
DOI: https://doi.org/10.2138/am-2018-6599

**Table 1**. EPMA data for the type nuwaite and butianite, associated Ge-bearing alloys and heazlewoodite in Allende.

| Constituent wt% | Nuwaite n=5[a] | Butianite n=4 | Alloy 1 n=5 | Alloy 2 n=4 | Heazlewoodite n=6 |
|---|---|---|---|---|---|
| Ni | 65.3(0.3)[b] | 62.1(0.7) | 72.6(0.8) | 78.0(0.7) | 68.5(0.8) |
| Fe | 1.72(0.07) | 1.3(0.2) | 10.0(0.2) | 10.8(0.3) | b.d. |
| Ge | 8.2(0.2) | 5.3(0.2) | 2.7(0.6) | 2.68(0.06) | b.d. |
| Sn | 5.10(0.03) | 11.1(0.2) | b.d. | b.d. | b.d. |
| S | 10.3(0.2) | 8.9(0.1) | b.d. | b.d. | 26.7(0.1) |
| Te | 7.9(0.2) | 10.3(0.2) | b.d. | b.d. | b.d. |
| Co | b.d.[c] | b.d. | 1.6(0.2) | 0.8(0.2) | b.d. |
| Pt | b.d. | b.d. | 4.5(0.3) | b.d. | b.d. |
| Ru | b.d. | b.d. | 0.4(0.1) | b.d. | b.d. |
| Total | 98.5 | 99.1 | 91.8[d] | 92.3[d] | 95.2[d] |
| No. of aroms | 9 | 9 | 1 | 1 | 5 |
| Ni | 5.95 | 5.93 | 0.82 | 0.84 | 2.92 |
| Fe | 0.16 | 0.13 | 0.12 | 0.12 | |
| Ge | 0.60 | 0.41 | 0.02 | 0.02 | |
| Sn | 0.23 | 0.52 | | | |
| S | 1.72 | 1.56 | | | 2.08 |
| Te | 0.33 | 0.45 | | | |
| Co | | | 0.02 | 0.01 | |
| Pt | | | 0.02 | | |
| Ru | | | 0.00 | | |

[a] n=number of analyses.
[b] Errors given inside parentheses are one standard deviation of the mean based on all of the analyses.
[c] b.d. = below detection limit: 0.2 wt% Fe, 0.1 wt% Fe, 0.1 wt% Sn, 0.1 wt% S, 0.1 wt% Te, 0.3 wt% Co, 0.2 wt% Pt, 0.1 wt% Ru.
[d] The low totals are due to small grain sizes.

This is a preprint, the final version is subject to change, of the American Mineralogist (MSA)
Cite as Authors (Year) Title. American Mineralogist, in press.
DOI: https://doi.org/10.2138/am-2018-6599

553 (a)

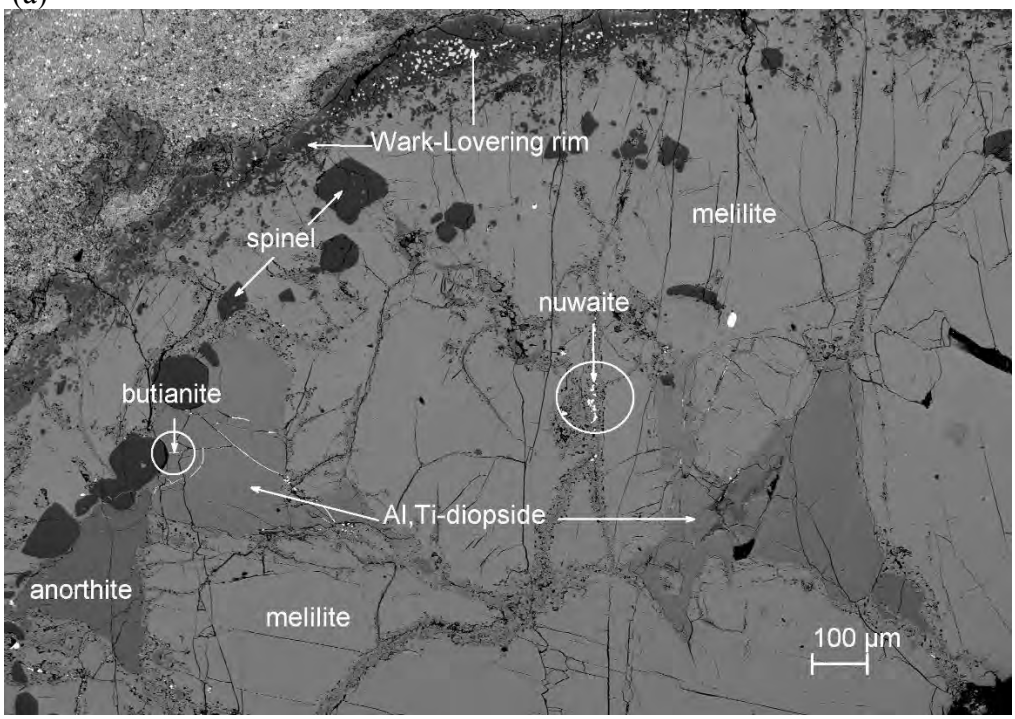


554
555 (b)

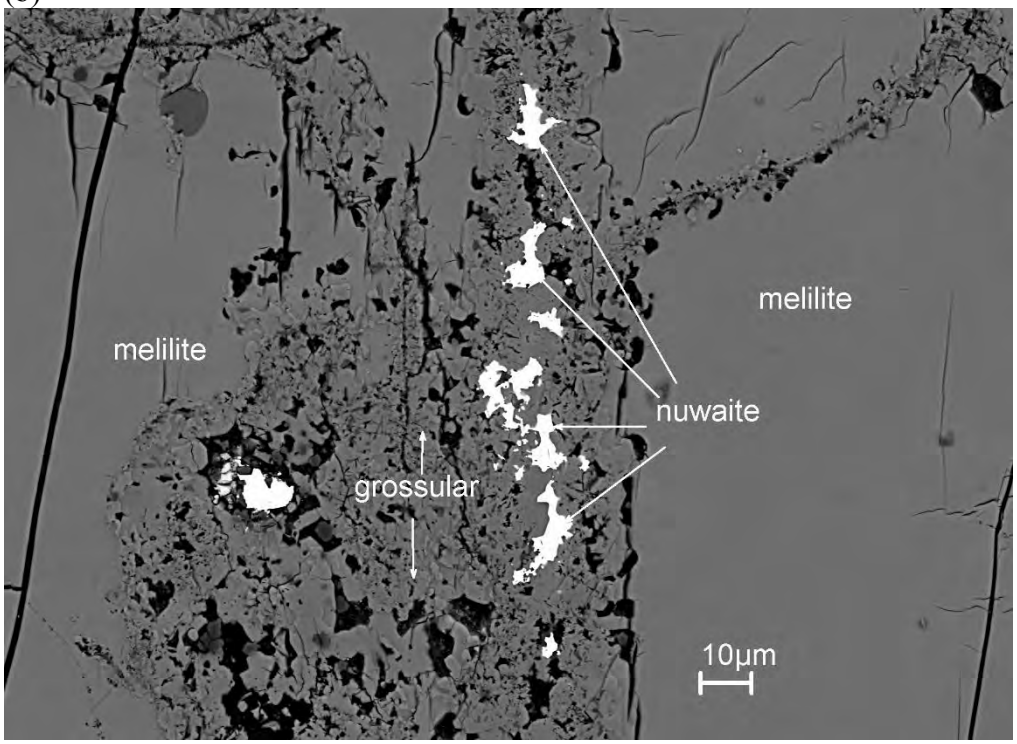


556
557

(c)

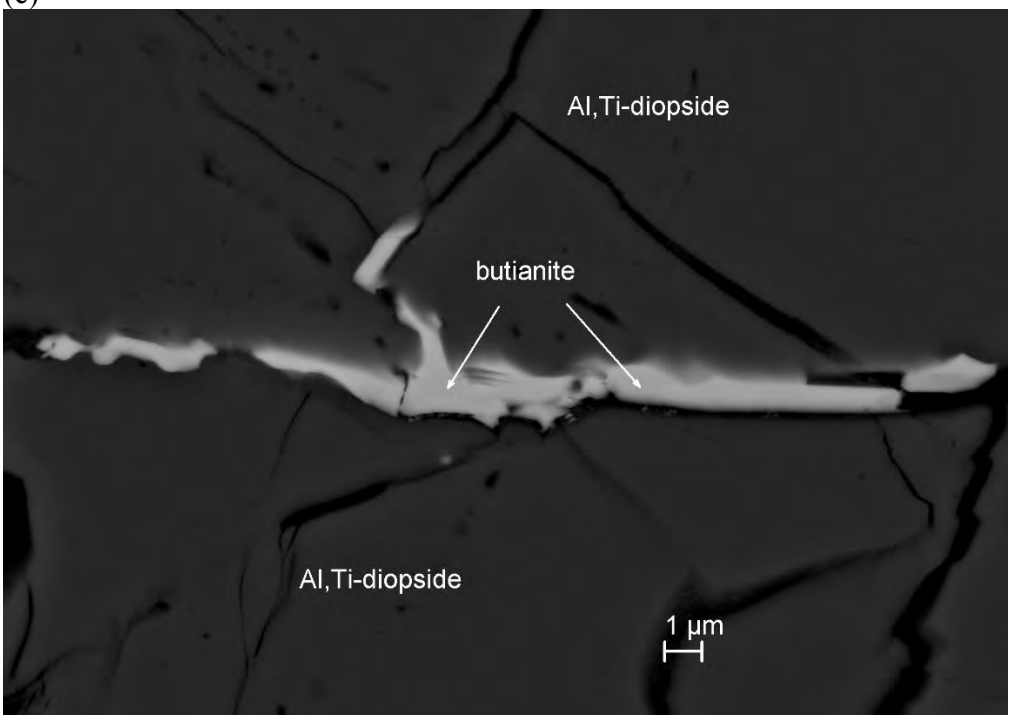


**Figure 1**. (a) Back-scatter electron (BSE) image showing part of the Type B1 CAI *ACM-2* in USNM 7616 with locations of type nuwaite and butianite indicated. (b) Enlarged BSE image showing nuwaite coexisting with grossular in an alteration vein in melilite. (c) BSE image showing type butianite filling a crack in Al,Ti-rich diopside.

This is a preprint, the final version is subject to change, of the American Mineralogist (MSA)
Cite as Authors (Year) Title. American Mineralogist, in press.
DOI: https://doi.org/10.2138/am-2018-6599

568 Fig. 2. (a)

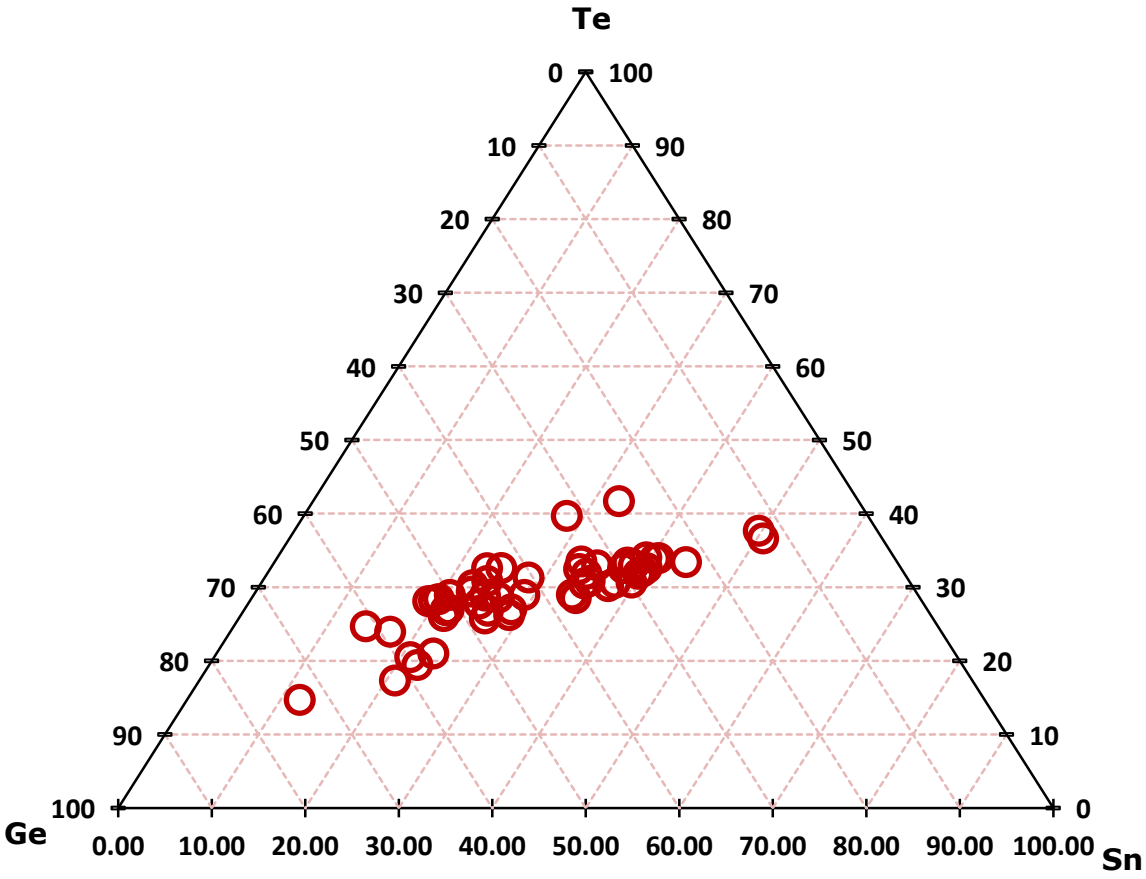


569

570

This is a preprint, the final version is subject to change, of the American Mineralogist (MSA)
Cite as Authors (Year) Title. American Mineralogist, in press.
DOI: https://doi.org/10.2138/am-2018-6599

571 Fig. 2. (b)

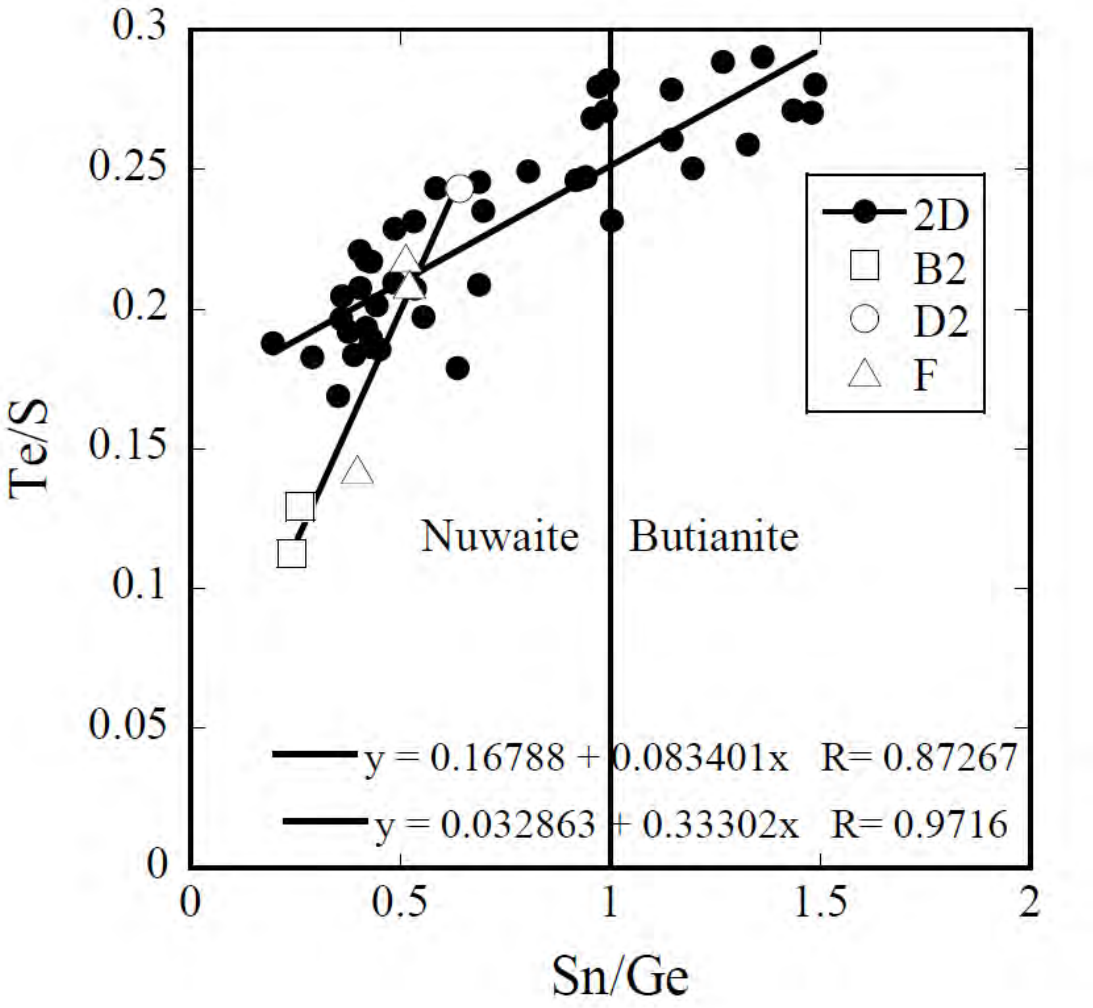


572

573

This is a preprint, the final version is subject to change, of the American Mineralogist (MSA)
Cite as Authors (Year) Title. American Mineralogist, in press.
DOI: https://doi.org/10.2138/am-2018-6599

574 Fig. 2. (c)

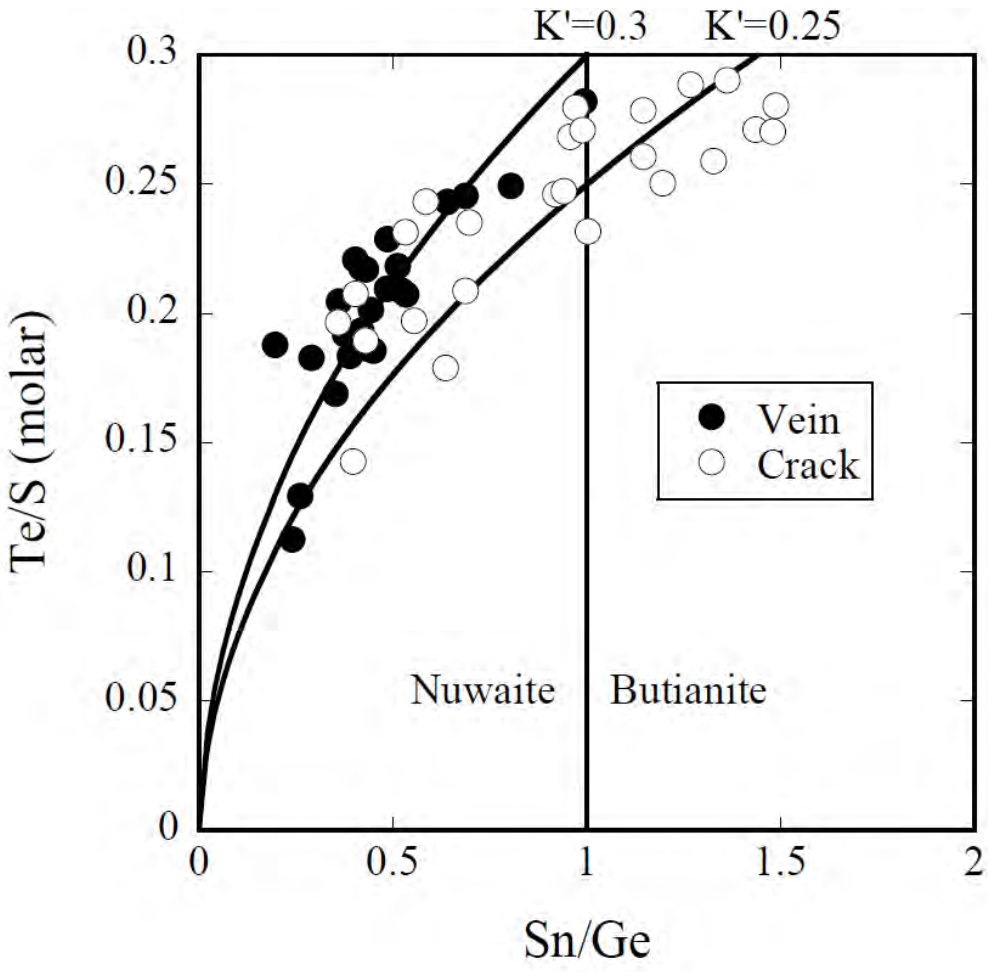


575

576 **Figure 2**. Nuwaite - butianite compositions (molar) in terms of (a) the Ge-Sn-Te ternary, (b)
577 Sn/Ge versus Te/S with compositions coded by section, and (c) Sn/Ge versus Te/S with
578 compositions coded by occurrence in grossular-rich vein or in cracks in pyroxene.

579

This is a preprint, the final version is subject to change, of the American Mineralogist (MSA)
Cite as Authors (Year) Title. American Mineralogist, in press.
DOI: https://doi.org/10.2138/am-2018-6599

(a) Nuwaite

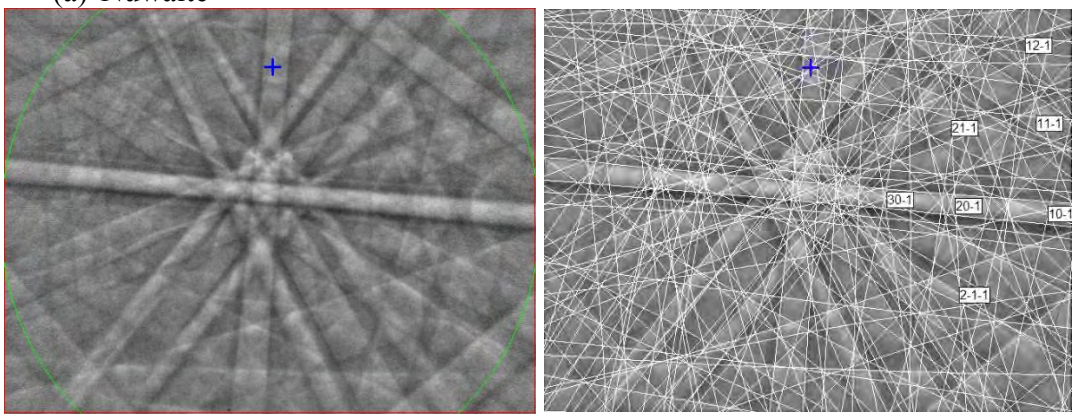


(b) Butianite

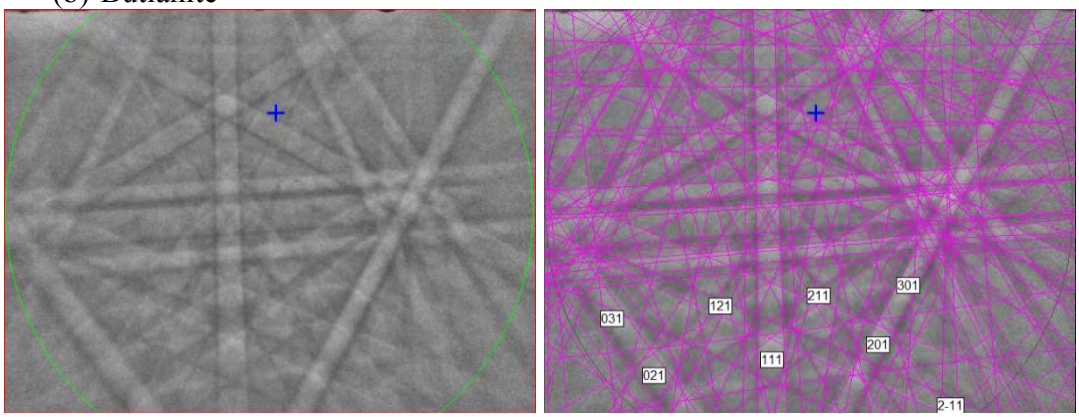


**Figure 3**. EBSD patterns (left) indexed with the *I4/mmm* $Ni_6SnS_2$ structure (right) for (a) type nuwaite crystal in Fig. 1b and (b) the type butianite crystal in Fig. 1c. Crosses indicate the center of a pattern.